THE JOURNAL OF PHYSICAL CHEMISTRY B

Article

pubs.acs.org/JPCB

Ion Segregation in Aqueous Solutions

Hongtao Bian,[†,∥] Jiebo Li,[†,∥] Qiang Zhang,[‡] Hailong Chen,[†] Wei Zhuang,*[,‡] Yi Qin Gao,*[,§] and Junrong Zheng*[,†]

[†]Department of Chemistry, Rice University, Houston, Texas 77005, United States

[‡]State Key Laboratory of Molecular Reaction Dynamics, Dalian Institute of Chemical Physics, Chinese Academy of Sciences, Dalian 116023, Liaoning, People's Republic of China

[§]College of Chemistry and Molecular Engineering, Beijing National Laboratory for Molecular Sciences, Peking University, Beijing 100871, China

Supporting Information

ABSTRACT: Microscopic structures and dynamics of aqueous salt solutions were investigated with the ultrafast vibrational energy exchange method and anisotropy measurements. In KSCN aqueous solutions of various concentrations, the rotational time constants of SCN^- anions are proportional to the viscosities of the solutions. However, the reorientation dynamics of the water molecules are only slightly affected by the solution viscosity. With the addition of strongly hydrated F^- anions, the rotations of both SCN^- anions and water molecules slow down. With the addition of weakly hydrated I^- anions, only the rotation of SCN^- anions slows down with that of water molecules unaffected. Vibrational energy exchange measurements show that the separation among SCN^- anions decreases with the addition of F^- and increases with the addition of I^-. The series of experiments clearly demonstrate that both structures and dynamics of ion and water are segregated in the strong electrolyte aqueous solutions.

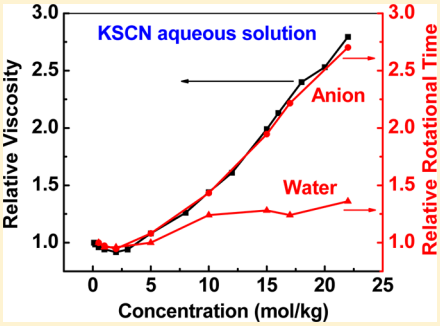

1. INTRODUCTION

Many chemical and most biological processes in nature proceed in aqueous electrolyte solutions,[1] the properties of which have been intensively studied for many years.[2−9] For very dilute solutions, electrolyte solutions can be well described by the Debye−Huckel theory.[10] However, this theory begins to fail for quite dilute solutions (even 10^{-3} M solutions with multiple-charged ions). Many practical situations, e.g., fuel cells, batteries, formations of natural mineral compounds, and salt crystallizations, involve much higher concentrations.[11] As solutions become more concentrated, the attractive forces between unlike ions overcome thermal agitation and condensed assemblies form. The complexity of this assembly process has drawn many research efforts to decipher it, but many open questions concerning the microscopic structures and dynamics of concentrated aqueous solutions remain.[2,12−19]

In the past decades, ultrafast infrared spectroscopy has been frequently used to probe the structures and dynamics of water molecules, ions, and solvent−solute interactions in electrolyte aqueous solutions.[20−34] Efforts have been focused on the measurements of reorientation, chemical exchange and spectral diffusion dynamics of water molecules in electrolyte aqueous solutions or in confined environments.[16,17,35,36] These previous studies have revealed many important aspects of water dynamics, e.g., it has been concluded that the presence of interfaces in aqueous solutions can change the dynamics of water molecules on the interfaces.[16,17,35,36] However, because of the lack of probe for the other component (ions) of the solutions, these studies have not been able to provide knowledge about the structural distribution of ions and the dynamical changes induced by such a distribution in the aqueous solutions.

In this work, by monitoring the anisotropy decays of vibrational excitation signals of both water molecules and anions, we were able to determine the rotational diffusion dynamics of both water molecules and SCN^- anions in a series of 1:1 strong electrolyte (KSCN and its mixtures with KF, KI, K_2CO_3 and K_2HPO_4) aqueous solutions. By monitoring the vibrational energy transfer kinetics[30,31,37,38] between SCN^- and $S^{13}C^{15}N^-$, we were able to determine the relative anion distances in the solutions. We obtained through these experiments clear evidence that both dynamical segregations and ion clusters exist in the unsaturated strong electrolyte aqueous solutions. Our molecular dynamic simulations suggest that the observed dynamical segregations originate from the structural inhomogeneity of the solutions, which is dependent on the relative water affinities of the ions.

2. EXPERIMENTAL SECTION

Materials. $KS^{13}C^{15}N$ was purchased from Cambridge Isotope Laboratory and used without further purification. All other salts were purchased from Sigma-Aldrich and used

Received: October 15, 2012
Revised: November 25, 2012
Published: November 26, 2012

 © 2012 American Chemical Society

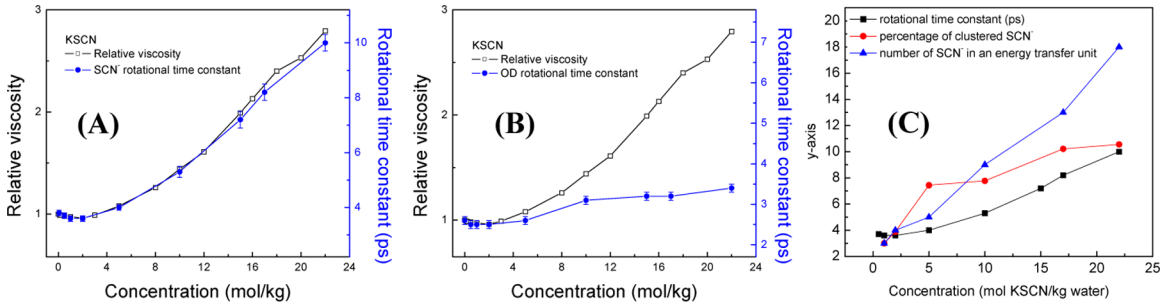

Figure 1. (A) The concentration-dependent viscosities (black) and rotational diffusion time constants of SCN^- anions (blue) of KSCN aqueous solutions. (B) The concentration-dependent viscosities (black) and rotational diffusion time constants of D_2O (blue) of KSCN aqueous solutions. The unit of concentration is mol (KSCN)/kg (water). (C) The concentration-dependent rotational diffusion time constants of SCN^- anions (black), percentage of clustered SCN^- anions (divided by 9, red), and number of anions in an vibrational energy transfer unit of an ion cluster (blue, which can be used to represent the fewest number of anions an ion cluster can have)[31] of KSCN aqueous solutions.

without further purification. D_2O was from C/D/N Isotopes Inc.

Experimental Methods. The optical setup is described previously.[37,39] Briefly, a picosecond (ps) amplifier and a femtosecond (fs) amplifier are synchronized with the same seed pulse. The ps amplifier pumps an OPA to produce ~1 ps Mid-IR pulses with a bandwidth 10−35 cm^{-1} in a tunable frequency range from 500 cm^{-1} to 4000 cm^{-1} with energy 1−40 μJ/pulse at 1 kHz. The fs amplifier pumps another OPA to produce ~140 fs Mid-IR pulses with a bandwidth ~200 cm^{-1} in a tunable frequency range from 600 cm^{-1} to 4000 cm^{-1} with energy 1−40 μJ/pulse at 1 kHz. In experiments, the ps IR pulse is the excitation beam. The fs IR pulse is the detection beam of which the frequencies are resolved by a spectrograph yielding the detection axis of a 2D IR spectrum. Scanning the excitation frequency yields the other axis of the spectrum. Two polarizers are inserted into the detection beam path to selectively measure the parallel or perpendicular polarized signal relative to the excitation beam. Vibrational lifetimes are obtained from the rotation-free 1−2 transition signal $P_{life} = P_{\parallel} + 2 \times P_{\perp}$, where $P_{\parallel}$ and $P_{\perp}$ are parallel and perpendicular signal respectively. Rotational relaxation times are acquired from the waiting time-dependent anisotropy $R = (P_{\parallel} - P_{\perp})/(P_{\parallel} + 2 \times P_{\perp})$. Samples were contained in cells composed of two CaF_2 windows separated by a Teflon spacer. The thickness of the spacer was adjusted from 0.5 μm to 250 μm depending upon the optical densities. The experimental optical path and apparatus after the generation of mid-IR pulses were purged with CO_2- and H_2O-free clean air. All measurements were carried out at room temperature (22 °C). Viscosities were measured with a Cannon−Fenske kinematic viscosity tube.

In water reorientation dynamic measurements, the excitation and detection OD frequencies were set at the OD central frequency. To avoid the effect of resonance energy transfer on the anisotropy decay, HOD solutions (1 wt % D_2O in H_2O) were used to obtain the OD reorientation dynamics in the series of KSCN aqueous solutions. In the neat D_2O/H_2O (1 wt %) solution, the absorption peak of OD stretch is centered at around 2505 cm^{-1}. In the KSCN solutions, with the increase of electrolyte concentration, the central position of OD peak blue shifts. The concentration-dependent Fourier transform infrared (FTIR) spectra are shown in Figure S1. In the analyses of water reorientation dynamics, the heat effect from the OD vibrational relaxation was removed, following the procedure described in our previous publication.[30] Solutions in D_2O with various $KS^{13}C^{15}N$/KSCN (= 2%) concentrations were used to conduct the SCN^- rotation anisotropy measurements. The FTIR spectra of KSCN showing the nitrile stretch are displayed in Figure S2 (Supporting Information). The OD and SCN^- anisotropy decay data are displayed in Figure S3 and tabulated in Table S1.

Molecular Dynamics Simulation Method. The widely used SPC/E model was adopted for the calculations of water. The parameters of KSCN, F^-, and I^- are listed in Table S7. In the calculations, each cubic box was filled with water molecules, and ions which were inserted randomly. The numbers of water molecules and ions in the simulation boxes are listed in Table S8. The geometries of water molecules and SCN^- anions were kept rigid. The Lorentz−Berthelot rules were used for the combined LJ parameters. The temperature was weakly coupled to a bath with the Nose-Hoover thermostats at 298 K with the relaxation time of 0.1 ps. The weak coupling Berendsen scheme was used to control the pressure with the coupling time constant of 1 ps. The equations of motion were integrated using the leapfrog algorithm with a time step of 2 fs. The long-range Coulombic forces were treated with the Ewald summation method. The nonbonded van der Waals interactions were truncated at 12 Å using the force shifting method. Minimum image conditions were used. For each run, one 5-ns NPT ensemble equilibration was followed by a 10-ns NVE ensemble simulation used to calculate the dynamic properties. Prior to this step, several quenching simulations were carried out in order to reach equilibration for each solution. The simulation trajectories were saved every 100 fs. The coordination number for each pair atom was characterized by the geometric criteria ($R_{X\text{-}Y}$< 3.5 Å for Ow−Ow, Ow−N, Ow−S, Ow−K, S−K, and N−K pairs). All simulations were performed with the Tinker simulation code.[40]

3. RESULTS AND DISCUSSION

3.1. Concentration Dependent Rotational Dynamics of SCN^- Anions and Water Molecules in KSCN Aqueous Solutions. Figure 1A,B displays the salt concentration-dependent viscosities (left axis) and rotational diffusion time constants (right axis) of SCN^- anions and D_2O in KSCN aqueous (D_2O) solutions. Below the concentration of 5 mol KSCN/kg water, the viscosity values and rotational time constants of both SCN^- and D_2O are almost unchanged. However, at higher concentrations, the rotational dynamics of anions and water become very different. As the viscosity increases 3-fold, the rotation of anions also slows about 3-fold, but water rotation slows only about 35%.

dx.doi.org/10.1021/jp310153n | J. Phys. Chem. B 2012, 116, 14426−14432

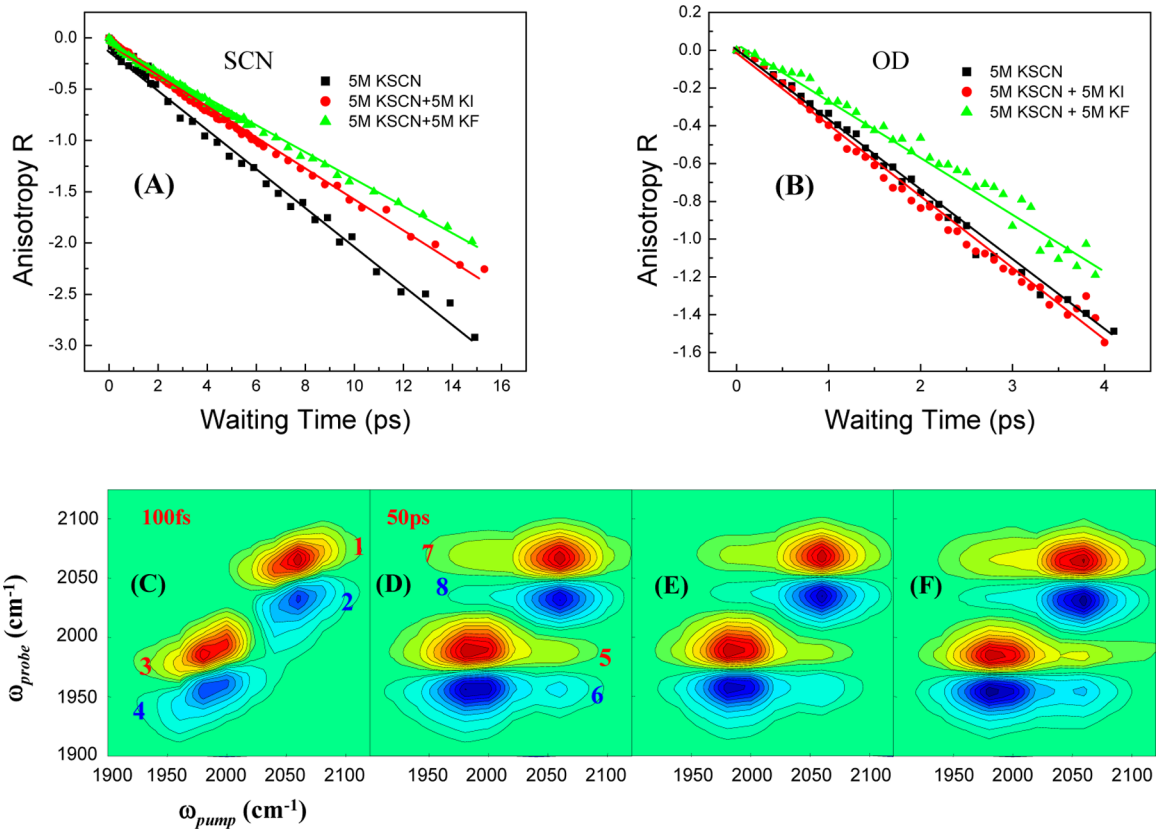

Figure 2. Logarithmic plots of anisotropy R as a function of delay time of a (5 mol KSCN)/kg aqueous solution, a (5 mol KSCN+ 5 mol KI)/kg aqueous solution, and a (5 mol KSCN+ 5 mol KF)/kg aqueous solution measured at (A) the SCN^- frequency region and (B) the OD frequency region. All the data are fitted to single exponential (solid line). Adding I^- into the KSCN solution slows down the rotational dynamics of SCN^- anions but not those of the water molecules. Adding F^- into the KSCN solution slows down the rotational dynamics of both SCN^- anions and water molecules. (C,D) 2D IR spectra of the (2.5 mol KSCN + 2.5 mol $KS^{13}C^{15}N$)/kg aqueous solution at waiting times of 100 fs and 50 ps. (E) 2D IR spectrum of the (2.5 mol KSCN + 2.5 mol $KS^{13}C^{15}N$ + 5 mol KI)/kg aqueous solution at a waiting time of 50 ps. (F) 2D IR spectrum of the (2.5 mol KSCN + 2.5 mol $KS^{13}C^{15}N$ + 5 mol KF) /kg aqueous solution at a waiting time of 50 ps. The growth of the cross peaks 5, 6, 7, and 8 indicates how fast vibrational energy transfers between SCN^- and $S^{13}C^{15}N^-$.

At lower concentrations (0−2 mol/kg), the normalized viscosity of the KSCN aqueous solution decreases slightly from 1 (the absolute value of normalized viscosity 1 is 0.97 centistokes) to 0.96 with the increase of KSCN concentration. This phenomenon has been observed for decades.[41] Its origin is generally believed to be that both K^+ and SCN^- are weakly hydrated ions, which leads to faster molecular motions, and a negative B coefficient as defined in the Jones−Dole equation for KSCN aqueous solutions.[3,42,43] Consistent with this explanation, we observed slightly speeded rotations of both SCN^- anions (3.8 ± 0.1 ps → 3.6 ± 0.1 ps) and water molecules (2.6 ± 0.1 ps → 2.5 ± 0.1 ps) with the increase of concentration from 0 to 2 mol/kg, as shown in Figure1A,B. In this series of experiments, the determination of individual rotational time has an uncertainty comparable to the change of rotational times. However, the relative difference among the rotational times of samples with different concentrations has a very small uncertainty, which allows us to clearly observe the concentration dependent trend.

At higher concentrations (>2 mol/kg), as determined previously[31] by the vibrational energy transfer method, a substantial fraction of KSCN ions form ion pairs and clusters. As shown in Figure 1C, as the concentration increases, more and bigger ion clusters form in the solutions.[31] SCN^- ions in bigger ion clusters have a slower angular velocity of rotation event if the velocity on the surface of the cluster remains constant. This effect could be interpreted as an increase of the local viscosity for SCN^- anions. Accordingly, the rotation of anions slows down. At the saturation concentration of KSCN, more than 90% of anions form big clusters.[31] Indeed, the rotational time constant (10 ± 0.3 ps) of SCN^- anions in the saturated solution approaches that of the anions in the KSCN crystal (11 ± 1 ps) at the same temperature (data are provided in the Supporting Information, Figure S4). For water molecules, the situation is reversed. At very low ion concentrations where water molecules are the majority, they rotate with the same velocity as bulk water, with a time constant of 2.6 ps.[13,20,35] With increasing ion concentration, a larger fraction of water molecules interact with the ions. The observed average water reorientational dynamics begin to approach those of the water molecules at the interfaces with the ions and ion clusters.[44]

3.2. F^- and I^- Have Different Effects on the Dynamics and Structures of KSCN Aqueous Solutions. The ion/water structural inhomogeneity and dynamic segregations in the KSCN aqueous solutions were also observed in mixed salt aqueous solutions. As displayed in Figure.2A,B (data in red), adding 5 mol KI into the 5 mol KSCN/kg aqueous solution slows down the rotational dynamics of the SCN^- anions from 4.2 ± 0.2 ps to 5.8 ± 0.3 ps (Figure 2A). However, the dynamics of water molecules are hardly affected by the addition of KI (Figure 2B), although the overall normalized viscosity of

dx.doi.org/10.1021/jp310153n | J. Phys. Chem. B 2012, 116, 14426−14432

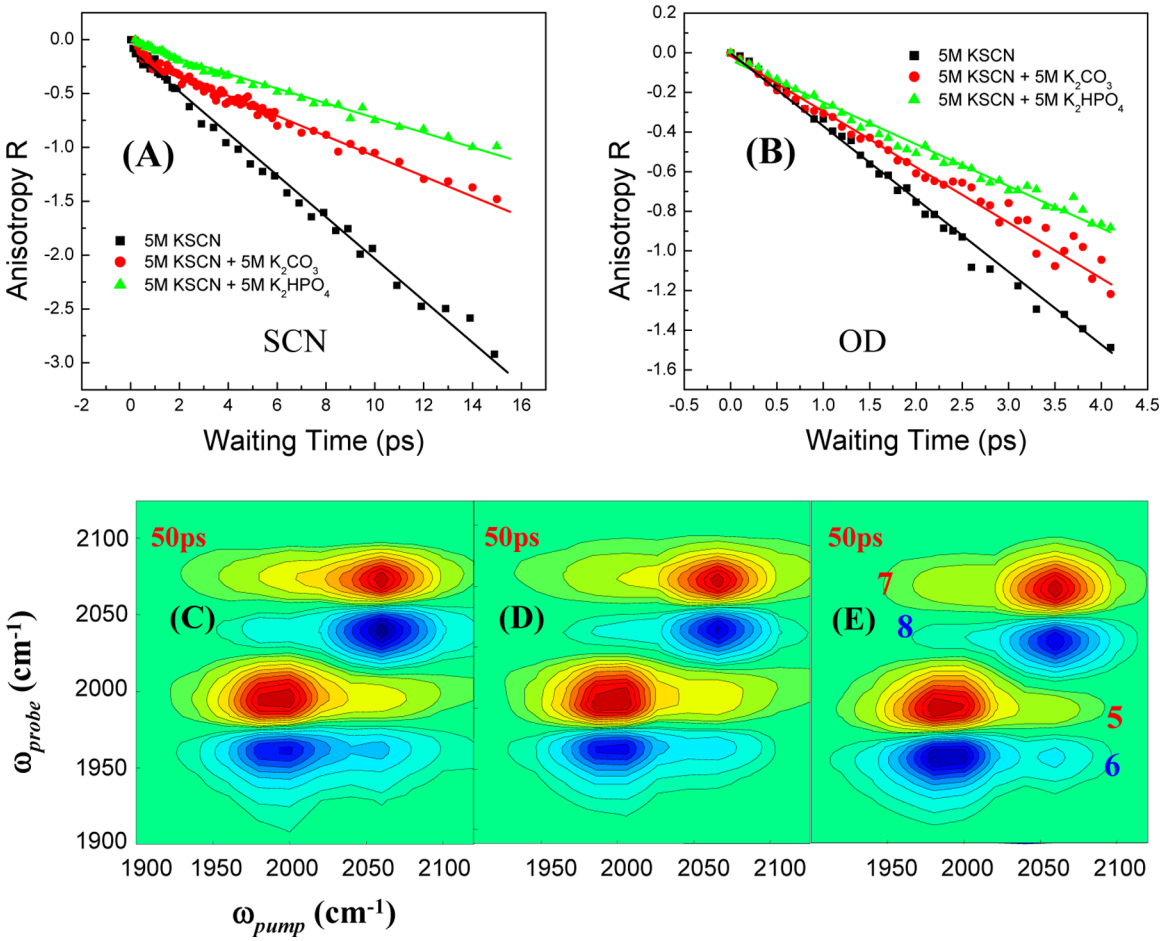

Figure 3. Logarithmic plots of anisotropy *R* as a function of delay time of a (5 mol KSCN)/kg aqueous solution, a (5 mol KSCN+ 5 mol K_2CO_3)/kg aqueous solution, and a (5 mol KSCN+ 5 mol K_2HPO_4)/kg aqueous solution measured at (A) the SCN^- frequency region and (B) the OD frequency region. All the data are fitted to single exponential (solid line). (C) 2D IR spectrum of the (2.5 mol KSCN + 2.5 mol $KS^{13}C^{15}N$ + 5 mol K_2CO_3)/kg aqueous solution at a waiting time 50 ps. (D) 2D IR spectrum of the (2.5 mol KSCN + 2.5 mol $KS^{13}C^{15}N$ + 5 mol K_2HPO_4)/kg aqueous solution at a waiting time 50 ps. (E) 2D IR spectrum of the (2.5 mol KSCN + 2.5 mol $KS^{13}C^{15}N$)/kg aqueous solution at a waiting time of 50 ps (identical to Figure 2D).

the solution increases from ~1.08 (KSCN solution) to ~1.35 (KSCN/KI mixed solution). These observations suggest that I^- anions associate with SCN^- anions. The likely association of I^- and SCN^- was further confirmed by the slowed vibrational energy transfer among the SCN^- anions upon the addition of KI as observed in 2D IR vibrational energy exchange measurements (Figure 2E). In explanation of Figure 2E, the vibrational energy transfer between SCN^- and $S^{13}C^{15}N^-$ in the (2.5 mol KSCN + 2.5 mol $KS^{13}C^{15}N$)/kg aqueous solution produces cross peaks in the 2D IR spectra (Peaks 5, 6, 7, and 8 in Figure 2D). A smaller cross peak (with fewer contours) indicates a smaller energy transfer rate. Figure 2E,D shows that adding 5 mol KI into the potassium thiocyanate solution produces a slightly smaller cross peaks compared to those before the addition, indicative of a slower energy transfer among the thiocyanate anions caused by the addition of KI. The detailed energy transfer kinetics and data analysis for the series of KSCN solutions are provided in the Supporting Information, Figures S6–S12. As elaborated in previous publications,[31,38] according to the dipole/dipole approximation of which the energy transfer rate is inversely proportional to the sixth power of donor/acceptor distance,[45] slower energy transfer results from a decrease in the population of thiocyanate anions in close contact (clustered) in the solution, if the transition dipole moments of the energy donor and acceptor and the local refractive index remain constant. Experiments show that the latter two factors change for less than 2% by the addition of 5 M KI (see Supporting Information Tables S3 and S4). After normalization to take into account the changes in these two factors, the energy transfer rate slows by 10% ± 2% in Figure 2E. This corresponds to ~10% concentration decrease of the closely contacted thiocyanate anions or to increased separation between the SCN^- ions. These calculations are provided in the Supporting Information, Tables S5 and S6.

In contrast to the results caused by the addition of KI, adding 5 mol of KF into the 5 mol KSCN/kg aqueous solution changes the rotational dynamics of both SCN^- anions and water molecules. The rotations of both water (from 2.6 ± 0.1 ps to 4.0 ± 0.2 ps) and SCN^- anions (from 4.2 ± 0.2 ps to 7.4 ± 0.3 ps) are slowed down by the addition of KF, as shown in Figure 2 A,B (data in green). It is well-known that, in contrast with I^- anions, F^- anions are strongly hydrated.[46,47] The strong binding between F^- anions and water molecules slows the rotational dynamics of water as observed, a behavior similar to that observed for other strongly hydrated ions (Li^+, Na^+, CO_3^{2-}, and SO_4^{2-}) in this and other studies.[23] Because of its strong water affinity, F^- can also out compete the weakly

dx.doi.org/10.1021/jp310153n | J. Phys. Chem. B 2012, 116, 14426–14432

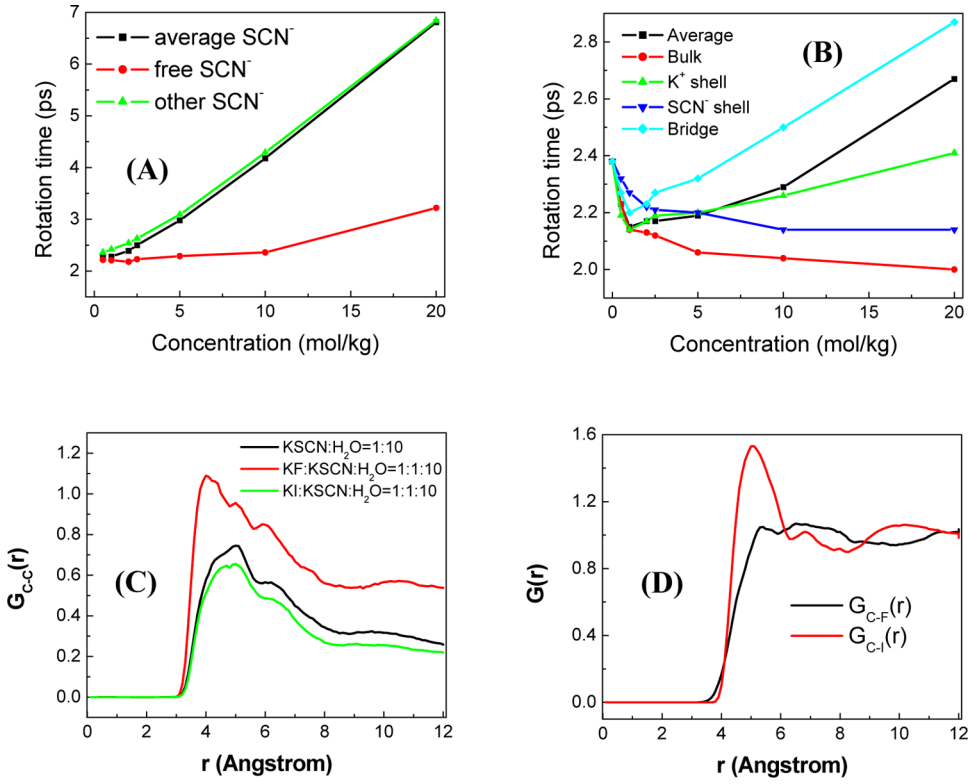

Figure 4. MD simulation results: (A) The rotational time constants of free SCN^- anions of which the first solvation shell contains only water molecules, and other SCN^- anions of which the first solvation shell contains at least one ion, and the average SCN^- rotational time constants of KSCN solutions at different KSCN concentrations. (B) The rotational time constants of water molecules of different microscopic environments in the KSCN solutions: (1) bulk, of which the first solvation shell is full of water; (2) K^+ shell, of which the first solvation shell has only one K^+ cation and water molecules; (3) SCN^- shell, of which the first solvation shell has only one SCN^- anion and water molecules; (4) bridge, of which the first solvation shell has at least two ions. (C) The C−C RDFs inside the KSCN ion clusters in the 5 mol/kg KSCN aqueous solution, in the 5 mol/kg KSCN aqueous solution added with 5 mol KF, and in the 5 mol/kg KSCN aqueous solution added with 5 mol KI. (D) The C−F RDF of the 5 mol/kg KSCN aqueous solution added with 5 mol KF, and the C−I RDF of the 5 mol/kg KSCN aqueous solution added with 5 mol KI.

hydrating SCN^- for water molecules in the mixed solution in which there are not sufficient water molecules to solvate each ion (the ion/water molar ratio is 1/2.5). This will reduce the number of water molecules solvating SCN^- anions, resulting in more SCN^- clustering in the mixed solution. Both effects contribute to the observed slowing of SCN^- rotation. The formation of more and bigger SCN^- clusters deduced from the rotational dynamics measurements was further supported by the observed faster vibrational energy exchange among the SCN^- anions from the vibrational energy exchange measurements (Figure 2F). The addition of 5 mol KF to the (2.5 mol KSCN + 2.5 mol $KS^{13}C^{15}N$)/kg aqueous solution produces energy exchange cross peaks with higher intensity (about one more contour in peak 6) (Figure 2F), compared to those (Figure 2D) of the solution before the KF addition. The result indicates that the addition of KF facilitates the energy transfer between SCN^- and $S^{13}C^{15}N^-$ anions, opposite to the effect of the addition of KI.

The experimental results described above qualitatively conclude that in the mixed aqueous solutions, I^- anions associate more with SCN^- clusters, but F^- anions associate more with water molecules. Our MD simulations provide a more quantitative picture about the conclusion. In the KSCN/KI mixed solution, our MD simulations show that 98% of the I^- anions have at least one K^+ in their first solvation shell, and 89% of these K^+ cations have at least one SCN^- in their first solvation shell. In other words, 87% (=98% × 89%) of the I^- anions are associated to SCN^- anions through K^+. No I^- is found to be in direct contact with SCN^-. In the KSCN/KF mixed solution, our MD simulations show that 41% of the F^- anions have at least one K^+ in their first solvation shell, and 66% of these K^+ cations have at least one SCN^- in their first solvation shell. In other words, only 27% (=41% × 66%) of the F^- anions are associated to SCN^- anions through K^+. No F^- is found to be in direct contact with SCN^-.

3.3. CO_3^{2-} and HPO_4^{2-} Have Similar Effects as F^-. The phenomenon that the weakly hydrated SCN^- anions are pushed closer to each other by the addition of strongly hydrated F^- anions was also observed when other strongly hydrated anions (CO_3^{2-} and HPO_4^{2-}) were added into the 5 mol KSCN/kg aqueous solution (Figure 3A−E). Similar to the addition of KF, with the addition of 5 mol of K_2CO_3 into the 5 mol KSCN/kg aqueous solution, the rotations of both SCN^- and water slow down from 4.2 ± 0.2 ps to 10.0 ± 0.3 ps (Figure 3A, data in red), and from 2.6 ± 0.1 ps to 3.8 ± 0.2 ps (Figure 3B, data in red), respectively. The addition of K_2HPO_4 also slows down the rotations of SCN^- and water, from 4.2 ± 0.2 ps to 13.0 ± 0.3 ps (Figure 3A, data in green), and from 2.6 ± 0.1 ps to 4.5 ± 0.2 ps (Figure 3B, data in green), respectively. The additions of these two anions also produce energy exchange cross peaks with about one more contour (peak 6 in Figure 3C,D) in 2D IR spectra, compared to those observed (Figure 3E or Figure 2D) for the pure potassium thiocyanate aqueous solution. These results indicate that the addition of these two

dx.doi.org/10.1021/jp310153n | J. Phys. Chem. B 2012, 116, 14426−14432

anions induces faster vibrational energy exchanges among SCN^- and $S^{13}C^{15}N^-$. As discussed above, the vibrational energy transfer rate in a solution is determined not only by the energy donor/acceptor distance, but also by the transition dipole moment of the donor and the acceptor, and the local refractive index. Our experiments and calculations show that adding 5 M of these different salts into the 5 M KSCN/kg−water solution changes the average transition dipole moment of the CN stretch of SCN^- and the average refractive indexes of the solutions by ≤2%. Normalized for the small changes of these two factors (details are provided in the Supporting Information), the energy transfer rate changes induced by the salt additions are slowed down 10% ± 2% by KI, accelerated 14% ± 2% by KF, accelerated 17% ± 2% by K_2CO_3, and accelerated 7% ± 2% by K_2HPO_4. According to the vibrational energy exchange model,[31] the normalized energy transfer rate changes correspond to the concentration changes of the direct contact thiocyanate anions: adding 5 M KI into the 5 M KSCN/kg-water solution reduced the concentration of energy-transfer-efficient (closely contact) thiocyanate anions from 67% ± 2% to 57% ± 2%. The concentration is increased to 76% ± 2% by the addition of KF, to 71% ± 2% by the addition of K_2HPO_4, and to 79% ± 2% by the addition of K_2CO_3. The small amount of hydroxyl anions produced by the hydrolysis of F^-, CO_3^{2-}, or HPO_4^{2-} is not responsible for the effect (faster energy transfer) observed. By contrast, adding 5 mol KOD into the thiocyanate solution slows down the energy exchange among the thiocyanate anions, similar to the effect of adding 5 M KI. Data are provided in the Supporting Information (Figure S12 and Table S2).

3.4. Molecular Dynamics Simulations. Molecular dynamics simulations provide further insights into the molecular pictures revealed by the experiments. As shown in Figure 4A,B, the rotations of both SCN^- anions and water molecules slow down at high ion concentrations (data in black). Similar to experimental observations, the rotational slowdown of SCN^- is much more significant than that of water. The experimentally observed slightly accelerated average rotations of water molecules at ∼2 mol/kg were reproduced from the MD simulations, but those of SCN^- anions were not. On the other hand, the simulations show that the free SCN^- anions of which the first solvation shell is full of water do rotate a little faster with the increase of concentration in the intermediate concentration range (data in red). The calculations also show that those anions that directly contact with at least one other ion (ion pairs and clusters, green data in Figure 4A) are the major components for the slower rotations at higher concentrations. The water molecules that make the major contribution to the slower rotation are those confined in the ion clusters and pairs (blue data in Figure 4 B), consistent with an earlier simulation study.[44] For the mixed salt solutions, calculations in Figure4C show that more SCN^- anions are in close contact (with the carbon−carbon distance <4 Å) with the addition of 5 mol KF into the 5 mol/kg KSCN aqueous solution (the red curve). By contrast, fewer SCN^- anions are within this distance range when KI is added (the blue curve), compared to those of the 5 mol/kg KSCN aqueous solution (the black curve). Because the energy transfer rate is inversely proportional to the sixth power of the donor/acceptor distance under the dipole approximation, these simulation results provide an explanation for the experimentally observed faster vibrational energy transfer rate by adding KF and the slower energy transfer rate by adding KI. Analyses of the C−I and C−F radial distribution functions (RDF) provide more insights for the interthiocyanate distance change caused by the salt additions. The C−I RDF in Figure 4D (the red curve) has a peak at ∼5 Å, indicating the direct contact between SCN^- and I^- (through K^+). Such a peak is absent in the C−F RDF in Figure 4D (the black curve), indicating that very few SCN^- are in direct contact with F^- (through K^+) in the mixed KSCN/KF aqueous solution. The MD simulations are in qualitative agreement with the experimental results, strongly supporting the existence of ion segregations in aqueous solutions. Whether the lack of quantitative agreement between experiment and simulation reflects limitations in our simulations awaits further investigation.

4. CONCLUDING REMARKS

Combining ultrafast anisotropy measurements, vibrational energy transfer measurements, and molecular dynamics simulations, we were able to observe distinct rotational behaviors of SCN^- anions and water molecules in a series of aqueous solutions containing KSCN and other potassium salts. The dynamical segregation of different components in the solutions reflects the structural inhomogeneity of the solutions. As deduced from the results of vibrational energy transfer measurements and MD simulations, ions form substantial amounts of ion clusters in the solutions. The structures and concentrations of ion clusters in the KSCN solutions mixed with other potassium salts are dictated by the nature of the added anions: (1) ions with high water affinities, e.g. F^-, and HPO_4^{2-}, tend to associate with water molecules and therefore reduce the number of water molecules solvating the KSCN ion clusters, promoting the formation of more KSCN ion clusters; and (2) ions with a low water affinity, e.g. I^-, tend to associate with the existing KSCN clusters. Because of the ion clustering, the local viscosity of the SCN^- anions is different from that of the water molecules, resulting in different rotational dynamics of the two components in the seemingly homogeneous electrolyte aqueous solutions.

■ ASSOCIATED CONTENT

Supporting Information

Supporting figures and data about FTIR spectra, anisotropy measurements, and data analyses. This material is available free of charge via the Internet at http://pubs.acs.org.

■ AUTHOR INFORMATION

Corresponding Author

*E-mail: junrong@rice.edu (J.Z.); wzhuang@dicp.ac.cn (W.Z.); gaoyq@pku.edu.cn (Y.Q.G.).

Author Contributions

‖These authors contributed equally to the work

Notes

The authors declare no competing financial interest.

■ ACKNOWLEDGMENTS

This material is based upon work supported by the Welch foundation under Award No. C-1752, and the Air Force Office of Scientific Research under AFOSR Award No. FA9550-11-1-0070. J.R.Z. also thanks the David and Lucile Packard Foundation for a Packard fellowship. W.Z. gratefully acknowledges the support of the NSFC QingNian Grant 21003117, NSFC key Grant 21033008 and Science and Technological Ministry of China Grant 2011YQ09000505. Y.Q.G. thanks the

NSFC for support (21125311 and 91027044). We also acknowledge Prof. Robert Curl's language modifications and suggestions on the manuscript.

REFERENCES

(1) Inman, D.; Lovering, D. G. *Ionic Liquids*; Plenum Press: New York/London, 1981.
(2) Marcus, Y.; Hefter, G. *Chem. Rev.* **2006**, *106*, 4585−4621.
(3) Marcus, Y. *Chem. Rev.* **2009**, *109*, 1346−1370.
(4) Buchner, R.; Hefter, G. *Phys. Chem. Chem. Phys.* **2009**, *11*, 8984−8999.
(5) Collins, K. D.; Neilson, G. W.; Enderby, J. E. *Biophys. Chem.* **2007**, *128*, 95−104.
(6) Collins, K. D. *Biophys. Chem.* **2006**, *119*, 271−281.
(7) Cacace, M. G.; Landau, E. M.; Ramsden, J. J. *Q. Rev. Biophys.* **1997**, *30*, 241−277.
(8) Jungwirth, P.; Tobias, D. J. *J. Phys. Chem. B* **2002**, *106*, 6361−6373.
(9) Zhang, Y. J.; Cremer, P. S. *Curr. Opin. Chem. Biol.* **2006**, *10*, 658−663.
(10) Debye, P.; Huckel, E. *Phys. Z.* **1923**, *24*, 185−206.
(11) Voigt, W. *Pure Appl. Chem.* **2011**, *83*, 1015−1030.
(12) Kropman, M. F.; Bakker, H. J. *Science* **2001**, *291*, 2118−2120.
(13) Park, S.; Odelius, M.; Gaffney, K. J. *J. Phys. Chem. B* **2009**, *113*, 7825−7835.
(14) Hassan, S. A. *J. Phys. Chem. B* **2008**, *112*, 10573−10584.
(15) Zavitsas, A. A. *J. Phys. Chem. B* **2001**, *105*, 7805−7817.
(16) Moilanen, D. E.; Wong, D.; Rosenfeld, D. E.; Fenn, E. E.; Fayer, M. D. *Proc. Natl. Acad. Sci. U.S.A.* **2009**, *106*, 375−380.
(17) Bakker, H. J. *Chem. Rev.* **2008**, *108*, 1456−1473.
(18) Laage, D.; Hynes, J. T. *J. Phys. Chem. B* **2008**, *112*, 7697−7701.
(19) Lin, Y. S.; Auer, B. M.; Skinner, J. L. *J. Chem. Phys.* **2009**, *131* (144511), 1−13.
(20) Omta, A. W.; Kropman, M. F.; Woutersen, S.; Bakker, H. J. *Science* **2003**, *301*, 347−349.
(21) Zheng, J.; Kwak, K.; Asbury, J. B.; Chen, X.; Piletic, I.; Fayer, M. D. *Science* **2005**, *309*, 1338−1343.
(22) Ji, M. B.; Odelius, M.; Gaffney, K. J. *Science* **2010**, *328*, 1003−1005.
(23) Tielrooij, K. J.; Garcia-Araez, N.; Bonn, M.; Bakker, H. J. *Science* **2010**, *328*, 1006−1009.
(24) Owrutsky, J. C.; Raftery, D.; Hochstrasser, R. M. *Annu. Rev. Phys. Chem.* **1994**, *45*, 519−555.
(25) Zhong, Q.; Baronavski, A. P.; Owrutsky, J. C. *J. Chem. Phys.* **2003**, *118*, 7074−7080.
(26) Sando, G. M.; Dahl, K.; Owrutsky, J. C. *J. Phys. Chem. A* **2004**, *108*, 11209−11217.
(27) Hamm, P.; Lim, M.; Hochstrasser, R. M. *J. Chem. Phys.* **1997**, *107*, 10523−10531.
(28) Ohta, K.; Tayama, J.; Tominaga, K. *Phys. Chem. Chem. Phys.* **2012**, *14*, 10455−10465.
(29) Lenchenkov, V.; She, C. X.; Lian, T. Q. *J. Phys. Chem. B* **2006**, *110*, 19990−19997.
(30) Bian, H. T.; Wen, X. W.; Li, J. B.; Zheng, J. R. *J. Chem. Phys.* **2010**, *133* (034505), 1−15.
(31) Bian, H. T.; Wen, X. W.; Li, J. B.; Chen, H. L.; Han, S.; Sun, X. Q.; Song, J.; Zhuang, W.; Zheng, J. R. *Proc. Natl. Acad. Sci. U.S.A.* **2011**, *108*, 4737−4742.
(32) Borek, J.; Perakis, F.; Klasi, F.; Garrett-Roe, S.; Hamm, P. *J. Chem. Phys.* **2012**, *136* (224503), 1−7.
(33) Kim, H.; Park, S.; Cho, M. *Phys. Chem. Chem. Phys.* **2012**, *14*, 6233−6240.
(34) van der Post, S. T.; Bakker, H. J. *Phys. Chem. Chem. Phys.* **2012**, *14*, 6280−6288.
(35) Fayer, M. D.; Moilanen, D. E.; Wong, D.; Rosenfeld, D. E.; Fenn, E. E.; Park, S. *Acc. Chem. Res.* **2009**, *42*, 1210−1219.
(36) Fayer, M. D. *Acc. Chem. Res.* **2012**, *45*, 3−14.
(37) Bian, H. T.; Li, J. B.; Wen, X. W.; Zheng, J. R. *J. Chem. Phys.* **2010**, *132* (184505), 1−8.
(38) Bian, H. T.; Chen, H. L.; Li, J. B.; Wen, X. W.; Zheng, J. R. *J. Phys. Chem. A* **2011**, *115*, 11657−11664.
(39) Chen, H. L.; Bian, H. T.; Li, J. B.; Wen, X. W.; Zheng, J. R. *Int. Rev. Phys. Chem.* **2012**, DOI: 10.1080/0144235X.2012.733116.
(40) Ponder, J. W.; Richards, F. M. *J. Comput. Chem.* **1987**, *8*, 1016−1024.
(41) Mitchell, J. P.; Butler, J. B.; Albright, J. G. *J. Sol. Chem.* **1992**, *21*, 1115−1129.
(42) Jenkins, H. D. B.; Marcus, Y. *Chem. Rev.* **1995**, *95*, 2695−2724.
(43) Marcus, Y. *J. Chem. Eng. Data* **2012**, *57*, 617−619.
(44) Yang, L. J.; Fan, Y. B.; Gao, Y. Q. *J. Phys. Chem. B* **2011**, *115*, 12456−12465.
(45) Woutersen, S.; Bakker, H. J. *Nature* **1999**, *402*, 507−509.
(46) Collins, K. D.; Washabaugh, M. W. *Q. Rev. Biophys.* **1985**, *18*, 323−422.
(47) Zhang, Y. J.; Cremer, P. S. Chemistry of Hofmeister Anions and Osmolytes. In *Annual Reviews Physical Chemistry*; Annual Reviews: Palo Alto, CA, 2010; Vol. *61*, pp 63−83.

Ion Segregation in Aqueous Solutions

Supporting Materials

Hongtao Bian[1†], Jiebo Li[1†], Qiang Zhang[2], Hailong Chen[1], Wei Zhuang[2*], Yi Qin Gao[3*], Junrong Zheng[1*]

1 Department of Chemistry, Rice University, Houston, TX 77005, USA

2 State Key Laboratory of Molecular Reaction Dynamics, Dalian Institute of Chemical Physics, Chinese Academy of Sciences, Dalian 116023, Liaoning, People's Republic of China

3 College of Chemistry and Molecular Engineering, Beijing National Laboratory for Molecular Sciences, Peking University, Beijing 100871, China

† These authors contribute equally to the work

* To whom correspondence should be addressed. E-mail: junrong@rice.edu, wzhuang@dicp.ac.cn, gaoyq@pku.edu.cn

FTIR spectra and anisotropy data

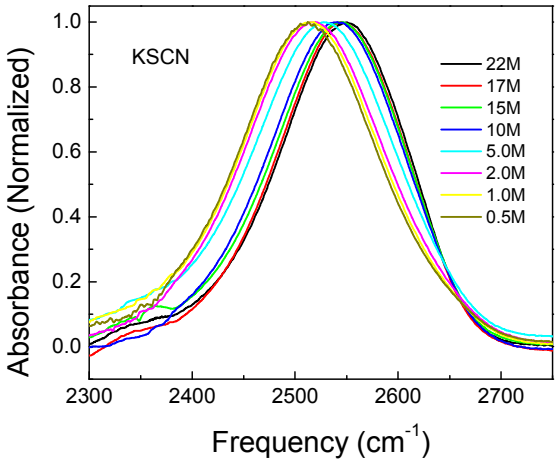

Figure S1. *FTIR spectra of KSCN aqueous solutions (HOD, 1 wt% D_2O in H_2O) in the OD stretch region with various KSCN concentrations. The concentration unit (M) is mol of KSCN/kg of water.*

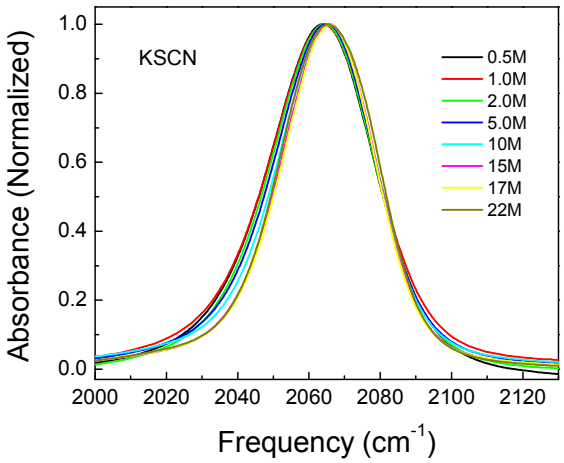

Figure S2. *FTIR spectra of KSCN aqueous solutions with various KSCN concentrations in the CN stretch 0-1 transition frequency region.*

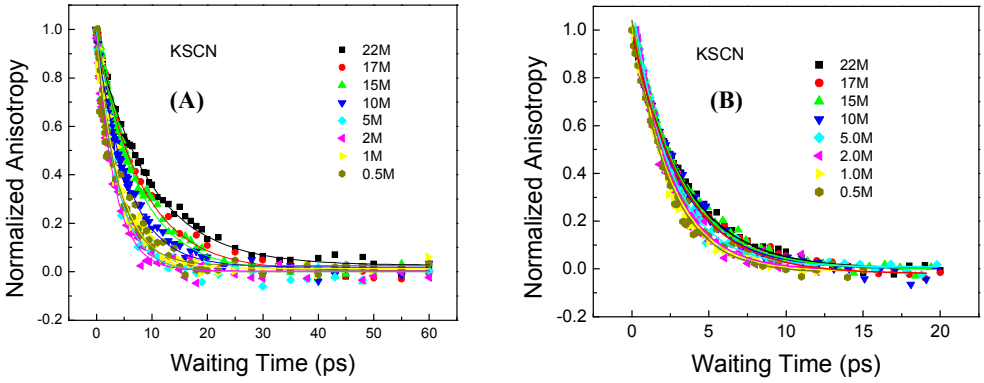

Figure S3. *Rotational relaxations of (A) SCN^- and (B) water of the KSCN aqueous solutions. Dots are the experimental results. Curves are the fitting results using single-exponential decays. Detailed fitting parameters are listed in Table S1.*

Table S1. Orientational relaxation parameters for the KSCN solution.

KSCN	τ_{SCN^-} (ps)	τ_{OD} (ps)
0	-	2.6±0.1
0.5M	3.8±0.1	2.5±0.1
1M	3.7±0.1	2.4±0.1
2M	3.6±0.1	2.4±0.1
5M	4.2±0.2	2.5±0.1
10M	5.3±0.2	3.1±0.2
15M	7.2±0.3	3.2±0.2
17M	8.2±0.3	3.1±0.2
22M	10.0±0.3	3.4±0.2

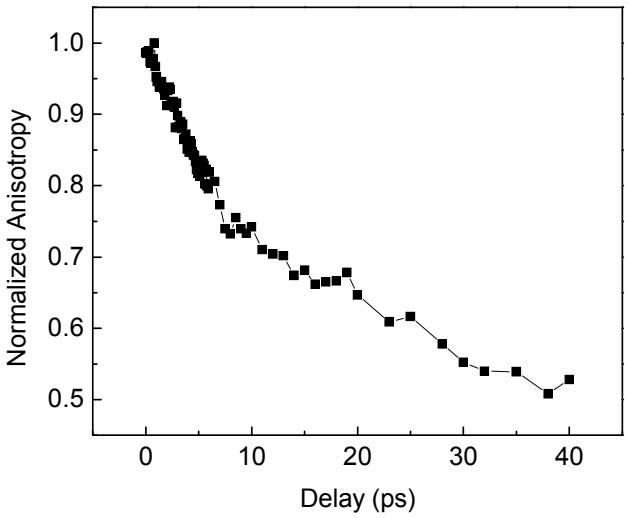

Figure S4. *Rotational anisotropy decay of $S^{13}C^{15}N^-$ in a KSCN/$KS^{13}C^{15}N$=98/2 (wt) mixed crystal. The rotational time constant was determined to be* $11 \pm 1 ps$. *The rotation is hindered in the crystal.*

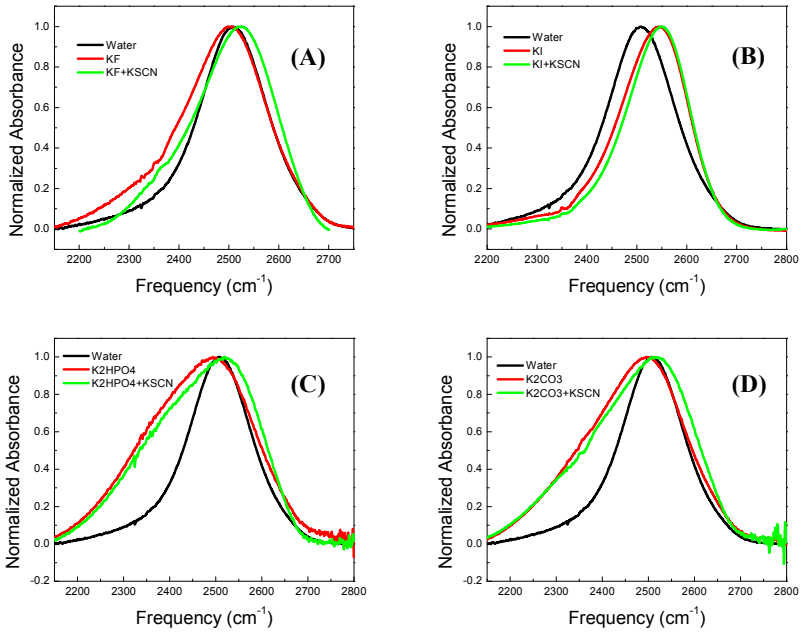

Figure S5. *FTIR spectra of solutions with different salts dissolved in the HOD solution (1 wt% D_2O in H_2O). (A) 5mol KF/1 kg water and (5mol KSCN+5mol KF)/1 kg water; (B) 5mol KI/1 kg water and (5mol KSCN+5mol KI)/1 kg water; (C) 5mol K_2HPO_4/1 kg water and (5mol KSCN+5mol K_2HPO_4)/1 kg water; (D) 5mol K_2CO_3/1 kg water and (5mol KSCN+5mol K_2CO_3)/1 kg water. In the solutions with KF, K_2CO_3, or K_2HPO_4, the hydroxyl anions from hydrolysis of the anions are broaden the OD stretch peak in the low frequency. The OD stretch tail at the low frequency range produces a small continuous absorption with descending amplitude with the decrease of frequency in 2D IR spectra at the frequency from 2080 cm^{-1} down to 1950 cm^{-1}. The 2D IR spectra shown in the main text were already compensated for this absorption.*

2D IR spectra normalization, correction and energy transfer kinetic analysis

In the main text, we use the cross peaks in 2D IR spectra (waiting time 50ps) to qualitatively represent the vibrational energy transfer rates between SCN^- and $S^{13}C^{15}N^-$ in different samples. Because the nitrile stretch vibrational lifetimes of SCN^- and $S^{13}C^{15}N^-$ are different in different solutions, the intensities of cross peaks (peaks 5&6) from raw data can't be directly used for comparison before normalization. We normalized the SCN^- diagonal peak pair (peaks 1&2) to be of the same intensity as the $S^{13}C^{15}N^-$ diagonal peak pair (peaks 3&4) at 50ps. The cross peak pair (peaks 5&6) was also normalized accordingly, using the same scaling factor (intensity ratio between peak 1 and peak 3). For the KSCN+KF, KSCN+K_2CO_3 and KSCN+K_2HPO_4 solutions, an additional blue peak which is probably due to the heat effect of the relaxation of OD stretch appears at frequencies from ~2400 cm^{-1} down to ~2060 cm^{-1} at long waiting times. The tail of this blue somewhat overlaps with red peak 1 and part of peak 1 intensity is cancelled. This causes the measured intensity of peak 1 in raw data is smaller than peak 2. To remove the overlapping effect, we corrected the peak intensities of peak 1 by assuming that the intensity ratio of peaks 1/2 at long waiting times is the same as those at short waiting times.

To quantitatively analyze the energy transfer kinetics between the two SCN^- stretches, we used a location-energy-exchange kinetic model which was shown in Scheme S1. In the model, vibrational energy can exchange between two closely contacted thiocyanate anions (SCN^-_{clu} and $S^{13}C^{15}N^-_{clu}$). Thiocyanate anions which are separated by water or other anions (SCN^-_{iso} and $S^{13}C^{15}N^-_{iso}$) can't exchange energy. The two types of thiocyanate anions can exchange locations. The vibrational energy of each species decays with its old lifetime. More details of the kinetic model were described in our previous publications.[1-3] From the kinetic model analysis, we can obtain the energy transfer rate constants, the equilibrium constant and the location exchange rate

constants. Detailed fitting parameters for the time dependent intensities of the diagonal peaks and the cross peaks of the mixed $KS^{13}C^{15}N$/KSCN aqueous solutions are shown in Figure S6 to S12. The results in Fig.S6~12 are to obtain the concentrations of clustered ions in different solutions with a fixed energy transfer time constant 140 ps for all solutions. The results are listed in Table S2. To compare the apparent energy transfer rates of the solutions, the concentrations of the clustered ions were taken to be the same in the calculations.

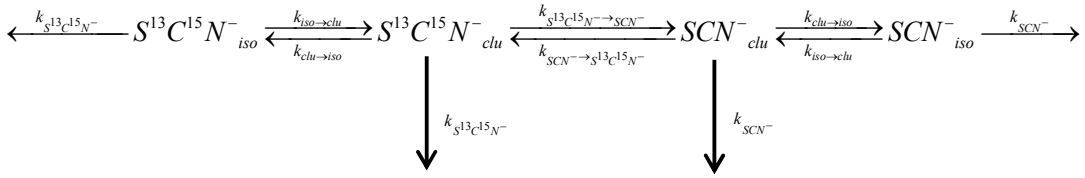

. (Scheme.S1)

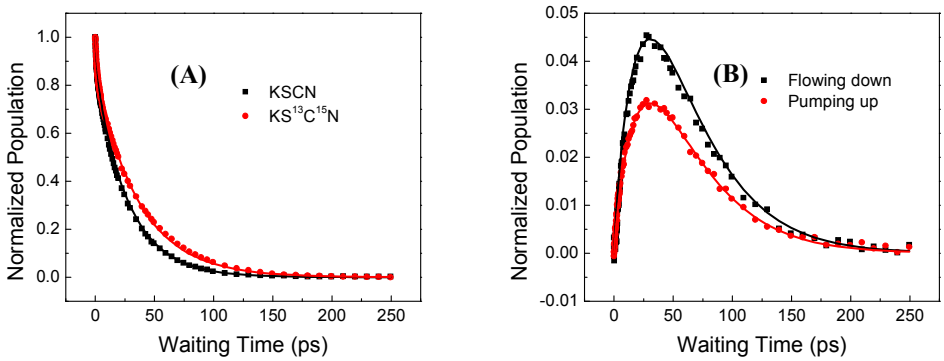

Figure S6. Data and calculations of nonresonance for $KS^{13}C^{15}N/KSCN/D_2O$ (0.5/0.5/10) aqueous solution. Dots are data, and lines are calculations. Calculations for (A) and (B) are with input parameters:

$k_{SCN^- fast} = 1/2.0\ (ps^{-1})$; $k_{SCN^- slow} = 1/28\ (ps^{-1})$; $k_{S^{13}C^{15}N^- fast} = 1/2.4\ (ps^{-1})$; $k_{S^{13}C^{15}N^- slow} = 1/35\ (ps^{-1})$;

$k_{clu \to iso} = 1/10\ (ps^{-1})$; K=2.0; $k_{SCN^- \to S^{13}C^{15}N^-} = 1/140\ (ps^{-1})$; D=0.7

with pre-factors of the subgroups and offset of the bi-exponential

$A_{SCN^- fast} = 0.04$; $A_{SCN^- slow} = 0.96$; $A_{S^{13}C^{15}N^- fast} = 0.15$; $A_{S^{13}C^{15}N^- slow} = 0.85$; $offset = 0$.

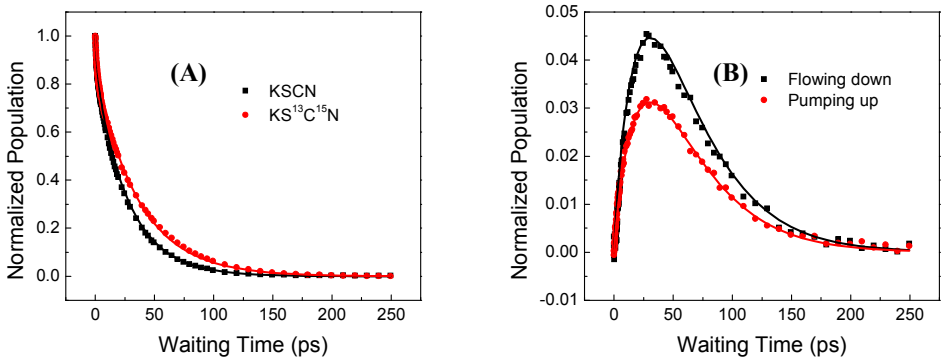

Figure S7. Data and calculations of nonresonance for $KS^{13}C^{15}N/KSCN/KF/D_2O$ (0.5/0.5/1/10) aqueous solution. Dots are data, and lines are calculations. Calculations for (A) and (B) are with input parameters:

$k_{SCN^- fast} = 1/2.0\ (ps^{-1})$; $k_{SCN^- slow} = 1/32\ (ps^{-1})$; $k_{S^{13}C^{15}N^- fast} = 1/2.6\ (ps^{-1})$; $k_{S^{13}C^{15}N^- slow} = 1/41\ (ps^{-1})$;

$k_{clu \to iso} = 1/10\ (ps^{-1})$; K=2.9; $k_{SCN^- \to S^{13}C^{15}N^-} = 1/140\ (ps^{-1})$; D=0.7

with pre-factors of the subgroups and offset of the bi-exponential

$A_{SCN^- fast} = 0.16$; $A_{SCN^- slow} = 0.84$; $A_{S^{13}C^{15}N^- fast} = 0.15$; $A_{S^{13}C^{15}N^- slow} = 0.85$; $offset = 0$.

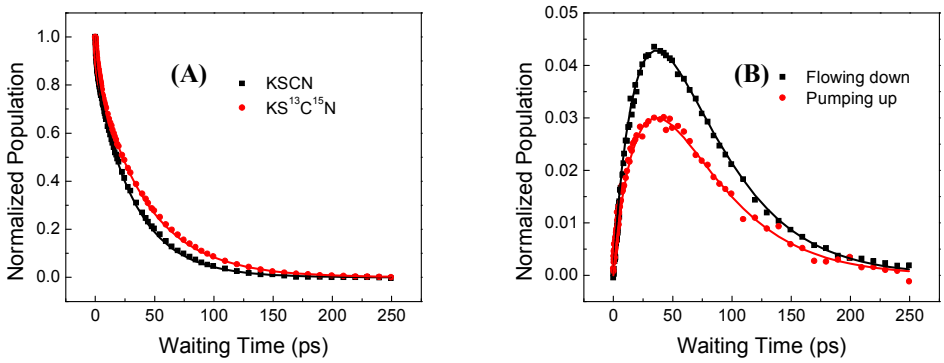

Figure S8. Data and calculations of nonresonance for $KS^{13}C^{15}N/KSCN/KI/D_2O$ (0.5/0.5/1/10) aqueous solution. Dots are data, and lines are calculations. Calculations for (A) and (B) are with input parameters:

$k_{SCN^- fast} = 1/2.0\ (ps^{-1})$; $k_{SCN^- slow} = 1/38\ (ps^{-1})$; $k_{S^{13}C^{15}N^- fast} = 1/2.6\ (ps^{-1})$; $k_{S^{13}C^{15}N^- slow} = 1/48\ (ps^{-1})$;

$k_{clu \to iso} = 1/10\ (ps^{-1})$; K=1.5; $k_{SCN^- \to S^{13}C^{15}N^-} = 1/140\ (ps^{-1})$; D=0.7

with pre-factors of the subgroups and offset of the bi-exponential

$A_{SCN^- fast} = 0.15$; $A_{SCN^- slow} = 0.85$; $A_{S^{13}C^{15}N^- fast} = 0.14$; $A_{S^{13}C^{15}N^- slow} = 0.86$; $offset = 0$.

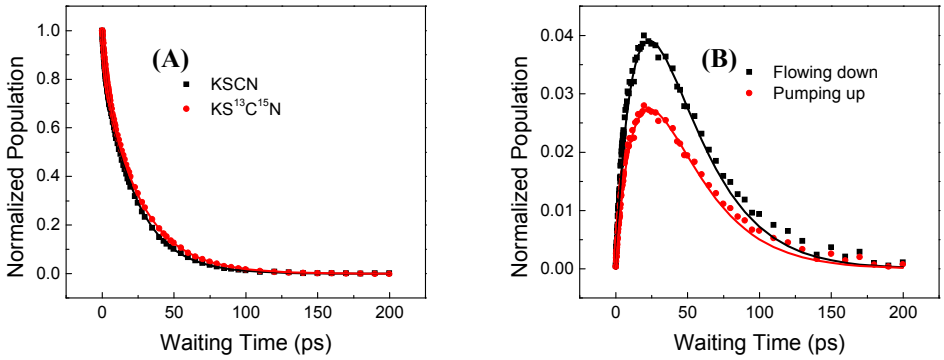

Figure S9. Data and calculations of nonresonance for $KS^{13}C^{15}N/KSCN/K_2CO_3/D_2O$ *(0.5/0.5/1/10)* aqueous solution. Dots are data, and lines are calculations. Calculations for (A) and (B) are with input parameters:

$k_{SCN^- fast} = 1/1.9\ (ps^{-1})$; $k_{SCN^- slow} = 1/26\ (ps^{-1})$; $k_{S^{13}C^{15}N^- fast} = 1/2.4 (ps^{-1})$; $k_{S^{13}C^{15}N^- slow} = 1/29\ (ps^{-1})$;

$k_{clu \to iso} = 1/10\ (ps^{-1})$; K=4.2; $k_{SCN^- \to S^{13}C^{15}N^-} = 1/140\ (ps^{-1})$; D=0.7

with pre-factors of the subgroups and offset of the bi-exponential

$A_{SCN^- fast} = 0.12$; $A_{SCN^- slow} = 0.88$; $A_{S^{13}C^{15}N^- fast} = 0.16$; $A_{S^{13}C^{15}N^- slow} = 0.84$; $offset = 0$.

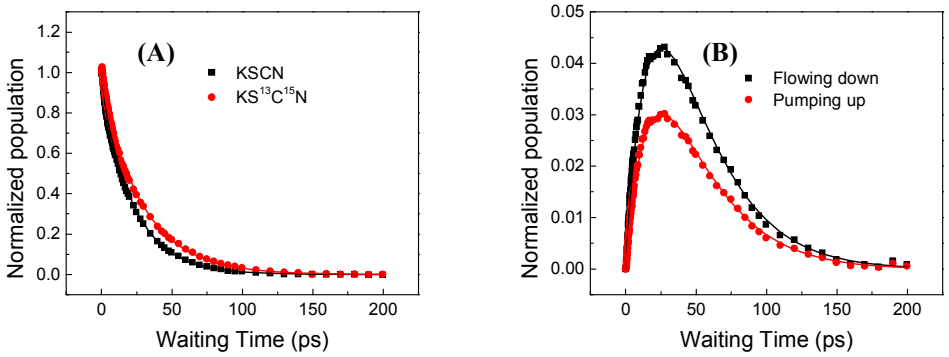

Figure S10. Data and calculations of nonresonance for $KS^{13}C^{15}N/KSCN/K_2HPO_4/D_2O$ (0.5/0.5/1/10) aqueous solution. Dots are data, and lines are calculations. Calculations for (A) and (B) are with input parameters:

$k_{SCN^-fast} = 1/1.0(ps^{-1})$; $k_{SCN^-slow} = 1/26.0\ (ps^{-1})$; $k_{S^{13}C^{15}N^-fast} = 1/1.5(ps^{-1})$; $k_{S^{13}C^{15}N^-slow} = 1/32.0(ps^{-1})$;

$k_{clu\to iso} = 1/10\ (ps^{-1})$; K=2.7; $k_{SCN^-\to S^{13}C^{15}N^-} = 1/140\ (ps^{-1})$; D=0.7

with pre-factors of the subgroups and offset of the bi-exponential

$A_{SCN^-fast} = 0.08;\ A_{SCN^-slow} = 0.98; A_{S^{13}C^{15}N^-fast} = 0.05;\ A_{S^{13}C^{15}N^-slow} = 0.95;\ offset = 0$.

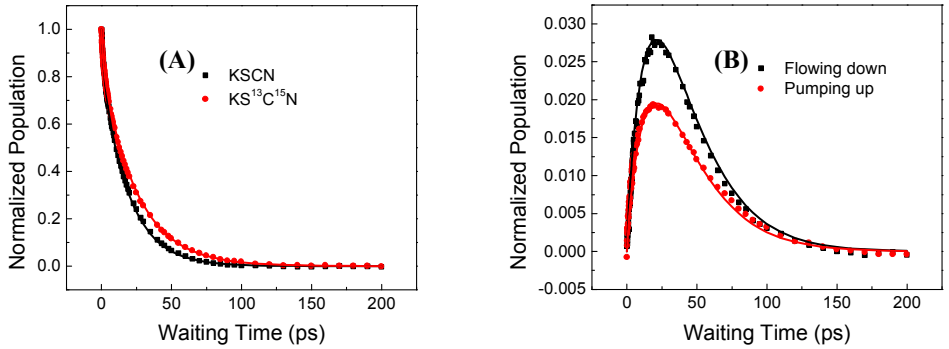

Figure S11. Data and calculations of nonresonance for $KS^{13}C^{15}N/KSCN/KOD/D_2O$ (0.5/0.5/0.2/10) aqueous solution. Dots are data, and lines are calculations. Calculations for (A) and (B) are with input parameters:

$k_{SCN^-fast} = 1/1.9\ (ps^{-1})$; $k_{SCN^-slow} = 1/21\ (ps^{-1})$; $k_{S^{13}C^{15}N^-fast} = 1/1.4\ (ps^{-1})$; $k_{S^{13}C^{15}N^-slow} = 1/27\ (ps^{-1})$;

$k_{clu\to iso} = 1/10\ (ps^{-1})$; K=2.0; $k_{SCN^-\to S^{13}C^{15}N^-} = 1/140\ (ps^{-1})$; D=0.7

with pre-factors of the subgroups and offset of the bi-exponential

$A_{SCN^-fast} = 0.16;\ A_{SCN^-slow} = 0.84; A_{S^{13}C^{15}N^-fast} = 0.14;\ A_{S^{13}C^{15}N^-slow} = 0.86;\ offset = 0$

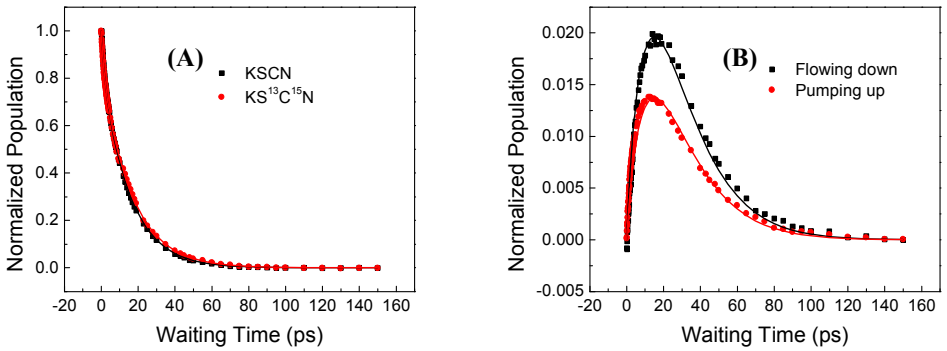

Figure S12. Data and calculations of nonresonance for $KS^{13}C^{15}N/KSCN/KOD/D_2O$ (0.5/0.5/1/10) aqueous solution. Dots are data, and lines are calculations. Calculations for (A) and (B) are with input parameters:

$k_{SCN^- fast} = 1/1.4\ (ps^{-1})$; $k_{SCN^- slow} = 1/16\ (ps^{-1})$; $k_{S^{13}C^{15}N^- fast} = 1/1.3\ (ps^{-1})$; $k_{S^{13}C^{15}N^- slow} = 1/17\ (ps^{-1})$;

$k_{clu \to iso} = 1/10\ (ps^{-1})$; K=1.7; $k_{SCN^- \to S^{13}C^{15}N^-} = 1/140\ (ps^{-1})$; D=0.7

with pre-factors of the subgroups and offset of the bi-exponential

$$A_{SCN^- fast} = 0.13;\ A_{SCN^- slow} = 0.87; A_{S^{13}C^{15}N^- fast} = 0.14;\ A_{S^{13}C^{15}N^- slow} = 0.86;\ offset = 0$$

Table S2. Concentrations of closely contacted SCN^- and $S^{13}C^{15}N^-$ in different samples with fixed energy transfer time constant 140 ps before the refractive index or transition dipole moment correction.

Samples	Cluster concentration
$KS^{13}C^{15}N/KSCN/D_2O$ *(0.5/0.5/10)*	$67 \pm 2\%$
$KS^{13}C^{15}N/KSCN/KI/D_2O$ *(0.5/0.5/1/10)*	$60 \pm 2\%$
$KS^{13}C^{15}N/KSCN/KF/D_2O$ *(0.5/0.5/1/10)*	$75 \pm 2\%$
$KS^{13}C^{15}N/KSCN/K_2CO_3/D_2O$ *(0.5/0.5/1/10)*	$81 \pm 2\%$
$KS^{13}C^{15}N/KSCN/K_2HPO_4/D_2O$ *(0.5/0.5/1/10)*	$73 \pm 2\%$
$KS^{13}C^{15}N/KSCN/KOD/D_2O$ *(0.5/0.5/0.2/10)*	$67 \pm 2\%$
$KS^{13}C^{15}N/KSCN/KOD/D_2O$ *(0.5/0.5/1/10)*	$63 \pm 2\%$

Transition dipole moment change measurements

The SCN^- stretch 0-1 transition dipole moment changes induced by the addition of $K_{1or2}X$(X=F, I, CO_3, HPO_4) were determined in the following procedure. KX salts and water were mixed with a certain molar ratio (1/10) to match that of the sample in 2D IR measurements. FTIR spectrum was taken from this mixture as the background. KSCN was then added into the mixture with a molar ratio 1/200 (KSCN/water). FTIR spectra of this sample and a solution KSCN/water (=1/200) were then measured. The density of each sample was measured to normalize the number of KSCN in the optical path. The change of the SCN^- transition dipole moment square is then proportional to the intensity change of SCN^- stretch peak 2065 cm^{-1} between samples with and without the addition of KX. The uncertainty of the measurements was estimated to be ~5%. The change given by this method is the maximum change the SCN^- stretch can have. In the 2D IR samples, because the KSCN concentration is much higher, the change is expected to be smaller. At the concentrations of the 2D IR samples, the FTIR measurements could not be reliably repeated because the very small optical path 1~2 microns. The measured $(\frac{\mu_{mixture}}{\mu_{KSCN}})^2$ s are listed in table S3.

Table S3. Transition dipole changes

Sample	$(\frac{\mu_{mixture}}{\mu_{KSCN}})^2$
KSCN/KF/H_2O (1/10)	1.03
KSCN/KI/H_2O (1/10)	0.98
KSCN/K_2CO_3/H_2O (1/10)	0.96
KSCN/K_2HPO_4/H_2O (1/10)	0.97

Refractive index correction

For the simplest condition, in the KSCN/KX/H_2O (1/1/10) mixed solutions, we assume 70% of the SCN^- anions are forming clusters, the rest of the SCN^- anions are hydrated by the solvent. Here the refractive index of the SCN^- clusters can be assumed the same as in the KSCN crystal (n=1.53). Then the refractive index of the mixed solution can be estimated using a linear expression

$$n_{mix} = 0.7 \times 1.53 + 0.3 \times n_{sol} \qquad \text{Eq. S1}$$

Here n_{sol} represents the refractive index of the solvent (water, n=1.33) and the cosolvent (KX, n_{sat}). For the same consideration, n_{sol} can also be described by a linear expression

$$n_{sol} = \frac{1}{11} \times n_{salt} + \frac{10}{11} \times 1.33 \qquad \text{Eq. S2}$$

The results of the refractive index for the different mixed solutions are displayed in Table S4.

Table S4. Refractive indexes of solutions

Salts	Refractive index n_{salt}	Solutions	Refractive index n_{sol}	Mixed solutions	Refractive index n_{mix}
KF	1.34	KF/H_2O=1/10	1.33	KSCN/KF/H_2O 1/1/10	1.47
KI	1.63	KI/H_2O=1/10	1.36	KSCN/KI/H_2O 1/1/10	1.48
K_2CO_3	1.53	K_2CO_3/H_2O=1/10	1.35	KSCN/K_2CO_3/H_2O 1/1/10	1.48
K_2HPO_4	1.48	K_2HPO_4/H_2O=1/10	1.34	KSCN/K_2HPO_4/H_2O 1/1/10	1.48

The Impacts of refractive index and transition dipole moment on the energy transfer rate

Under the dipole-dipole approximation, the energy transfer rate is proportional to the $\frac{\mu_{SCN}^4}{n^4}$. For the (2.5mol KSCN+2.5mol $KS^{13}C^{15}N$)/1 kg water solution, the energy transfer rate between the CN and $^{13}C^{15}N$ stretches was determined to be $\frac{1}{k} = 140\,ps$, and the closely contacted anion concentration was determined to be $67 \pm 2\%$.

First, we assume the energy transfer rates are the same in the mixed salts solution. Then the closely contacted concentrations can be obtained for the different mixed salts solutions accordingly. The concentrations are $75 \pm 2\%$, $60 \pm 2\%$, $81 \pm 2\%$ and $73 \pm 2\%$ for the KSCN/KF, KSCN/KI, KSCN/K_2CO_3 and KSCN/K_2HPO_4 mixed solutions, respectively. The corrected energy transfer rates and the cluster concentrations (after the correction with the transition dipole moment and the refractive index) are listed in Table S5.

Second, we assumed that in all the mixed salts solutions, the closely contacted SCN^- concentrations are the same, which is $67 \pm 2\%$. We then obtained their energy transfer time constant $\frac{1}{k}$: $125 \pm 3\,ps$, $155 \pm 3\,ps$, $113 \pm 3\,ps$ and $125 \pm 3\,ps$ for the KSCN/KF, KSCN/KI, KSCN/K_2CO_3 and KSCN/K_2HPO_4 mixed solutions, respectively. After corrected with the differences of the transition dipole moment and the refractive index, the corrected energy transfer rates results are listed in Table S6. We can see from both tables that the corrections don't change the trend at all. Only the detailed values are very slightly affected.

Table S5. Energy transfer rate and cluster concentration

Solutions	Energy transfer rate (1/k, ps)	Cluster concentration before correction	Cluster concentration after correction
KSCN/D_2O 1/10	140	$67 \pm 2\%$	$67 \pm 2\%$
KSCN/KF/D_2O 1/1/10	140	$75 \pm 2\%$	$76 \pm 2\%$
KSCN/KI/D_2O 1/1/10	140	$60 \pm 2\%$	$57 \pm 2\%$
KSCN/K_2CO_3/D_2O 1/1/10	140	$81 \pm 2\%$	$79 \pm 2\%$
KSCN/K_2HPO_4/D_2O 1/1/10	140	$73 \pm 2\%$	$71 \pm 2\%$

Table S6. Energy transfer rate and cluster concentration

Solutions	Cluster concentration	Energy transfer rate (1/k, ps)	Energy transfer rate correction (1/k, ps)
KSCN/D_2O 1/10	67%	$140 \pm 3 ps$	$140 \pm 3 ps$
KSCN/KF/D_2O 1/1/10	67%	$125 \pm 3 ps$	$120 \pm 3 ps$
KSCN/KI/D_2O 1/1/10	67%	$155 \pm 3 ps$	$154 \pm 3 ps$
KSCN/K_2CO_3/D_2O 1/1/10	67%	$113 \pm 3 ps$	$116 \pm 3 ps$
KSCN/K_2HPO_4/D_2O 1/1/10	67%	$125 \pm 3 ps$	$130 \pm 3 ps$

Molecular dynamics simulation details

The widely used SPC/E model was adopted for the calculations of water. The parameters of KSCN, F^- and I^- are listed in Table S7. In the calculations, each cubic box was filled with water molecules and ions which were inserted randomly. The numbers of water molecules and ions in the simulation boxes are listed in Table S8. The geometries of water molecules and SCN^- anions were kept rigid. The Lorentz-Berthelot rules were used for the current combined LJ parameters. The temperature was weakly coupled to a bath with the Nose-Hoover thermostats at 298 K with the relaxation time of 0.1 ps. The weak coupling Berendsen scheme was used to control the pressure with the coupling time constant of 1 ps. The equations of motion were integrated using the leapfrog algorithm with a time step of 2 fs. The long-range Coulombic forces were treated with the Ewald summation method. The non-bonded van der Waals interactions were truncated at 12 Å using the force shifting method. Minimum image conditions were used. For each run, one 5-ns NPT ensemble equilibration was followed by a 10-ns NVE ensemble simulation used to calculate the dynamic properties. Prior to this step, several quenching simulations were carried out in order to reach equilibration for each solution. The simulation trajectories were saved every 100 fs. The coordination number for each pair atom was characterized by the geometric criteria ($R_{X\text{-}Y}$< 3.5 Å for Ow-Ow, Ow-N, Ow-S, Ow-K, S-K, and N-K pairs). All simulations were performed with the Tinker simulation code.[4]

Table S7. The potential parameters

	Atom	*q* (e)	σ (Å)	ε(kJ·mol^{-1})
[5]SPC/E	Ow	-0.8476	3.166	0.650
water	Hw	0.4238	0.000	
	S	-.0.56	3.52	1.5225
[6]SCN^-	C	0.16	3.35	0.425
	N	-0.58	3.31	0.310
[7]K^+		+1.0	3.33	0.42
[8]F^-		-1.0	3.12	0.75
[8]I^-		-1.0	5.17	0.42

Table S8. The simulation bulk information

Concentration	Num of KSCN	Num of mixed ion	Num of water
0.5 mol	12		1176
1mol	24		1176
2mol	46		1154
2.5 mol	56		1122
5 mol	110		1090
10mol	200		1000
20mol	416		1000
1:1:10 (1mol KF)	110	110 (KF)	1090
1:1:10 (1mol KI)	110	110 (KI)	1090

References

(1) Bian, H. T.; Li, J. B.; Wen, X. W.; Zheng, J. R. *J. Chem. Phys.* **2010**, *132*, 184505, 1-8.

(2) Bian, H. T.; Wen, X. W.; Li, J. B.; Zheng, J. R. *J. Chem. Phys.* **2010**, *133*, 034505 1-15.

(3) Bian, H. T.; Wen, X. W.; Li, J. B.; Chen, H. L.; Han, S.; Sun, X. Q.; Song, J.; Zhuang, W.; Zheng, J. R. *Proc. Nat. Acad. Sci.* **2011**, *108*, 4737-4742.

(4) Ponder, J. W.; Richards, F. M. *J. Comput. Chem.* **1987**, *8*, 1016-1024.

(5) Berendsen, H. J. C.; Grigera, J. R.; Straatsma, T. P. *J. Phys. Chem.* **1987**, *91*, 6269-6271.

(6) Vincze A; Jedlovszky P; Horvai G. *Anal. Sci.* **2001**, *17*, i317.

(7) Lee, S. H.; Rasaiah, J. C. *J. Phys. Chem.* **1996**, *100*, 1420-1425.

(8) Chang, T. M.; Dang, L. X. *J. Phys. Chem. B* **1999**, *103*, 4714-4720.